Evaluation of Load-Displacement Relationships for Non-Slender Monopiles in Sand

Sørensen, Søren Peder Hyldal; Møller, M.; Brødbæk, K. T.; Augustesen, Anders Hust; Ibsen, Lars Bo

Publication date:
2009

Document Version
Publisher's PDF, also known as Version of record

Evaluation of Load-Displacement Relationships for Non-Slender Monopiles in Sand

S. P. H. Sørensen
M. Møller
K. T. Brødbæk
A. H. Augustesen
L. B. Ibsen

ISSN 1901-726X
DCE Technical Report No. 79

AALBORG UNIVERSITY
Department of Civil Engineering

Aalborg University
Department of Civil Engineering
Water & Soil

DCE Technical Report No. 79

Evaluation of Load-Displacement Relationships for Non-Slender Monopiles in Sand

by

S. P. H. Sørensen
M. Møller
K. T. Brødbæk
A. H. Augustesen
L. B. Ibsen

December 2009

Scientific Publications at the Department of Civil Engineering

Technical Reports are published for timely dissemination of research results and scientific work carried out at the Department of Civil Engineering (DCE) at Aalborg University. This medium allows publication of more detailed explanations and results than typically allowed in scientific journals.

Technical Memoranda are produced to enable the preliminary dissemination of scientific work by the personnel of the DCE where such release is deemed to be appropriate. Documents of this kind may be incomplete or temporary versions of papers—or part of continuing work. This should be kept in mind when references are given to publications of this kind.

Contract Reports are produced to report scientific work carried out under contract. Publications of this kind contain confidential matter and are reserved for the sponsors and the DCE. Therefore, Contract Reports are generally not available for public circulation.

Lecture Notes contain material produced by the lecturers at the DCE for educational purposes. This may be scientific notes, lecture books, example problems or manuals for laboratory work, or computer programs developed at the DCE.

Theses are monograms or collections of papers published to report the scientific work carried out at the DCE to obtain a degree as either PhD or Doctor of Technology. The thesis is publicly available after the defence of the degree.

Latest News is published to enable rapid communication of information about scientific work carried out at the DCE. This includes the status of research projects, developments in the laboratories, information about collaborative work and recent research results.

Published 2009 by
Aalborg University
Department of Civil Engineering
Sohngaardsholmsvej 57,
DK-9000 Aalborg, Denmark

Printed in Aalborg at Aalborg University

ISSN 1901-726X
DCE Technical Report No. 79

Evaluation of Load-Displacement Relationships for Non-Slender Monopiles in Sand

S. P. H. Sørensen; M. Møller; K. T. Brødbæk; A. H. Augustesen; and L. B. Ibsen

Abstract

Monopiles are an often used foundation concept for offshore wind turbine converters. These piles are highly subjected to lateral loads and bending moments due to wind and wave forces. To ensure enough stiffness of the foundation and an acceptable pile-head deflection, monopiles with diameters of 4 to 6 m are typically necessary. In current practice these piles are normally designed by use of the p–y curve method although the method is developed and verified for small-diameter, slender piles with diameters up to approximately 2 m. This paper investigate the behaviour of two non-slender aluminium pipe piles subjected to lateral loads at a given vertical eccentricity. The piles are heavily instrumented with strain gauges in order to obtain p–y curves and bending moment distributions along the piles. In order to minimise scale effects the tests are successfully carried out in a pressure tank at varying stress levels. The tests are evaluated with the following main findings: The lateral pile deflection consists primarily of rotation as a rigid object; normalised load-displacement relationships indicate that the lateral load is proportional to the embedded length squared and the pile diameter; in current design the initial stiffness of the p–y curves is considered independent of the pile diameter. This recommendation is questionable as derived p–y curves indicate a strong dependency on pile diameter with a higher initial stiffness related to the largest pile diameter.

Keywords: Non-slender monopiles, Lateral load, Laboratory tests, Pressure tank, Varying stress levels, p–y curves, Sand.

1 Introduction

In current design of laterally loaded monopiles, used as foundation for offshore wind turbines, the p–y curve method is normally employed. Two of the non-clarified parameters related to the expression for the p–y curves for piles in cohesionless soil is, cf. Brødbæk et. al (2009):

- Slenderness ratio L/D
- Initial stiffness of the p–y curves

Monopile foundations for modern offshore wind turbines have $L/D < 10$ and behave almost as rigid objects. In contrast the p–y curves employed in the design regulations, e.g. API (1993) and DNV (1992), are based on testing of two slender flexible piles with $L/D = 34.4$, cf. Cox et al. (1974).

The initial stiffness of the p–y curves is considered independent of the pile properties among these the pile diameter, which seems questionable. The research within the field of diameter effects gives contradictory conclusions, cf. Brødbæk et. al (2009).

This paper evaluates the listed effects through tests. Since large-scale tests are expensive and time consuming, small-scale tests are conducted. Small-scale tests are however attached to significant scale ef-

fects. When conducting small-scale tests in sand at 1-g an often introduced source of error is the low stress levels causing the soil parameters and in specific the angle of internal friction to vary strongly with effective stresses. Therefore, it is an advantage to increase the effective stresses to a level where the angle of internal friction is independent of a possible stress variation during the tests. Furthermore, an increase in effective stress level minimise fluctuations on the measured signals.

The problem for low stress levels can be overcome by testing piles in a centrifuge or in a pressure tank as described in section 2.

This paper presents the results obtained by testing horizontally loaded piles in sand in a pressure tank, cf. fig. 1, at various stress levels. The conducted tests are quasi-static tests on two instrumented closed-ended aluminium pipe piles with outer diameters of 60 mm and 80 mm, respectively. The outline of the paper is:

- **Pressure tank:** The test setup, including the method for increasing the stress level.
- **Measuring system:** The employed measurement devices and the preparation of the test piles.
- **Soil conditions:** Material properties of the sand and preparation of the soil prior to testing.
- **Results:** Interpretation of strain gauge measurements and a discussion of the obtained results.

2 Pressure tank

The tests have been carried out in the pressure tank shown in fig. 1 at Aalborg University, Denmark. A cross sectional view of the test setup is illustrated in fig. 2. The pressure tank is manufactured by Bergla Maskinfabrik in Brønderslev, Denmark. The diameter and the height of the pressure tank are approximately 2.1 m and 2.5 m, respectively. The pressure tank is installed in a load-frame, cf. fig. 1, resting on a reinforced foundation independent of the floor in the laboratory. On top of the pressure tank a platform, cf. fig. 1, is installed in order to make access to the top and hereby the preparation for the tests more comfortable. The pressure tank has trap doors, which make the preparation prior to the testing possible. Furthermore, the tank contains openings, cf. fig. 3, where the measurement devices are lead out. At the top hatch, cf. fig. 1, a hydraulic piston is mounted in order to install the test piles. The pressure tank contains 0.69 m of fully saturated sand, cf. fig. 2. A high permeable layer of gravel is located underneath the sand. The instrumented piles are actuated by a hydraulic piston, cf. fig. 1, and due to displacement transducers and a force transducer the load-displacement relationships at three levels above soil surface is obtained.

The increase in effective stress level is created by separating the lower part of the tank, containing saturated soil, from the upper part by use of an elastic membrane. In this way the saturated soil is sealed from the air above. By increasing the pressure in the upper part of the tank, a homogenous increase in stresses is introduced at the soil surface by the elastic membrane comparable to a surface load. To ensure limited excessive pore pressure, the soil is connected to an ascension pipe, leaving the soil fully saturated but with stresses applied as effective stresses only. The pile is lead through a sealing in the elastic membrane allowing the pile to be extended above the soil surface. An example of the variation of effective vertical stresses is shown in fig. 4, where P_0 denote the magnitude of the overburden pressure.

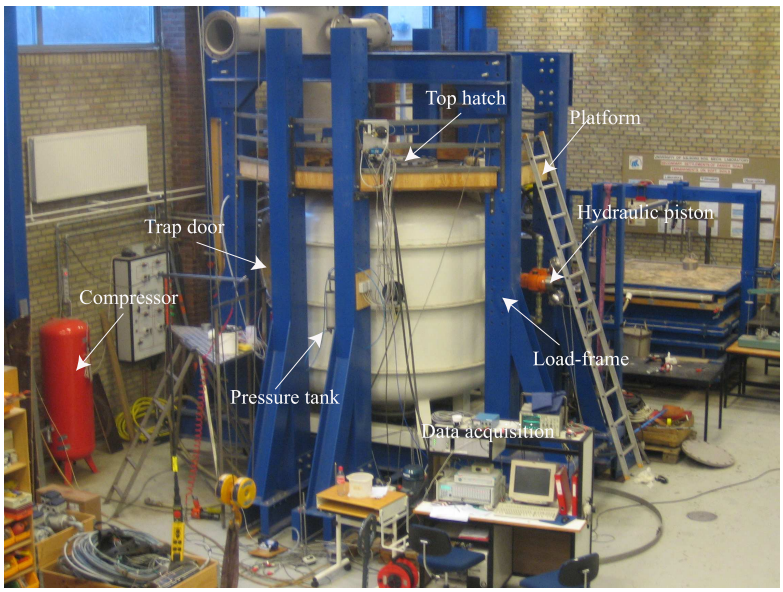

Figure 1: Pressure tank used for small-scale tests.

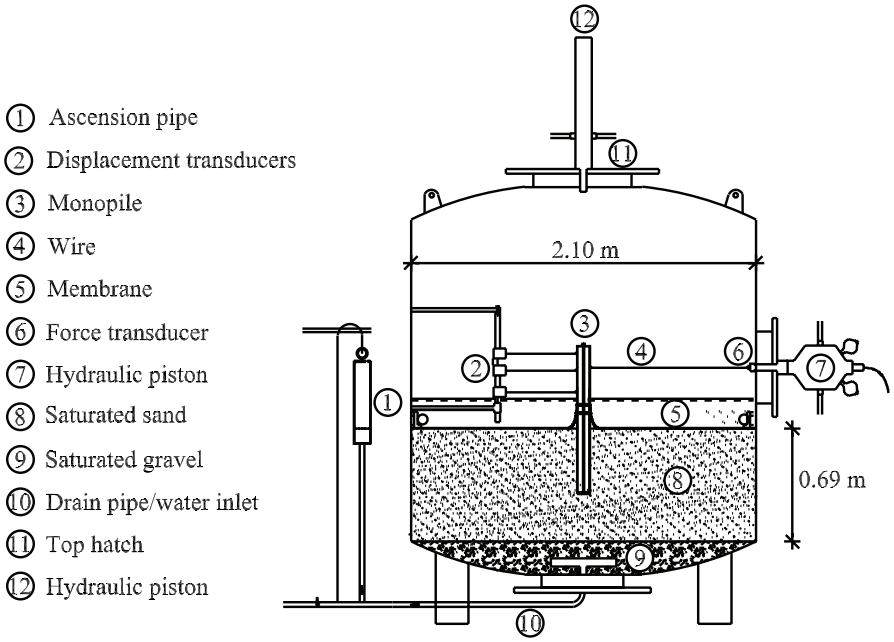

Figure 2: Test setup.

Figure 3: Openings for the measurement devices.

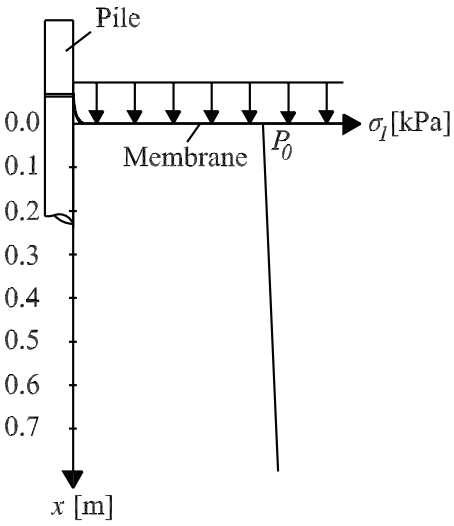

Figure 4: Variation of effective vertical stresses.

In the upper part of the pressure tank, approximately 16 cm of water is poured in, to ensure that the soil is fully saturated if leaks between the membrane and the pressure tank occurs. Further, the dynamic viscosity of water is about 55 times higher than in air[2], which minimise the flow through any potential gaps.

Due to the test setup, the maximum sand depth is 0.69 m. In order to minimise effects of the boundaries, piles with diameters of 0.08 m and 0.06 m and embedded lengths of 0.4 m and 0.3 m, respectively, are employed.

3 Measuring system

A hydraulic piston, cf. ⑦ in fig. 2, actuates the test piles. The hydraulic piston is controlled by a prescribed displacement and acts with a vertical eccentricity in the range of 0.370 – 0.375 m above the soil surface, cf. fig. 5. In order to measure the force acting on the pile a force transducer of the type HBM U2B 10 kN connects in series the hydraulic piston and the wire. Lateral displacements at three levels above the soil surface are measured, cf. fig. 5. In addition the vertical displacement is measured for the pile with an outer diameter of 60 mm. In order to measure the lateral and vertical displacement, displacement transducers of the type WS10-1000-R1K-L10 from ASM GmbH are employed. A total number of 10 strain gauges are mounted on the pile beneath the soil surface. The tank pressure is measured by a HBM P6A 10 bar absolute pressure transducer. The sampling frequency is 10 Hz.

3.1 Test piles

Two instrumented aluminium piles with outer diameters of 80 mm (6082 AW-

[2] http://www.lmnoeng.com/fluids.htm

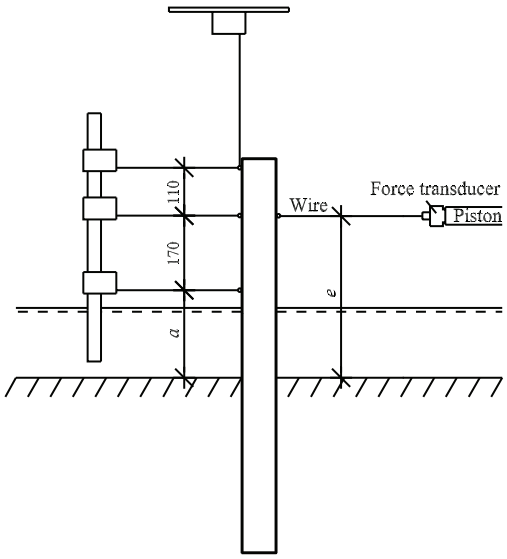

Figure 5: Measuring of lateral displacements at three levels, and measuring of the vertical displacement at the back of the pile. The distance a and the load eccentricity e are as listed in tab. 3.

6082/T6) and 60 mm (6060 AW-6060/T6) respectively, have been tested. Both piles have a wall thickness of 5 mm and are closed-ended in order to protect the strain gauges and their corresponding cords against water. The pile with an outer diameter of 80 mm is shown in fig. 6.

Figure 6: Picture of the test pile with an outer diameter of 80 mm. The cords are lead out through the blue cable.

The strain gauges are mounted at five levels as shown in fig. 7. At each level two foil strain gauges are mounted on the pile with a mutual angle of 180° aligned in the plane of the horizontal load as illustrated in fig. 8. The strain gauges are mounted in vertical direction implying that the curvature strains in the axial direction of the pile are measured. Strain gauges of the type HBM K-LY43-3/120 are employed, which are encapsulated strain gauges produced to measure on aluminium alloys.

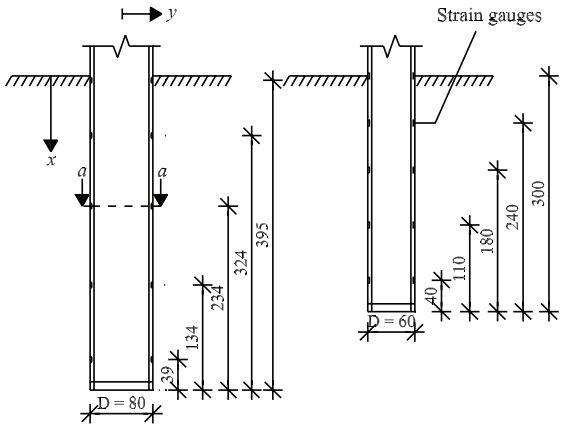

Figure 7: Strain gauge levels. Measures are in mm.

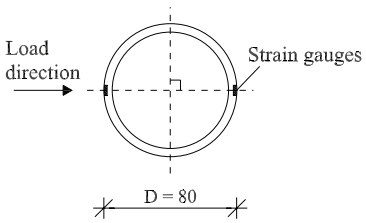

Figure 8: Cross section a–a. All measurement levels are identical. Measures are in mm.

The strain gauges are installed in milled grooves in the aluminium profile and sealed with a waterproofed filler (HBM SG250). In order to make the surface area around the grooves smooth a two component fast curing adhesive (HBM X60) is employed on the outside of the protective coating. The depth, width, and length of the mill outs are approximately 2, 6, and 10 mm, respectively. The weakening of the profiles as a consequence of this is negligible compared to the bending stiffness of the remaining profile. The gauges are bonded to the piles with a two-part epoxy. The cables from the strain gauges are lead into the pile and through a hermetic packed hole in the pile-head, cf. fig. 6.

3.1.1 Calibration of test piles

In order to ensure a proper relation between the strain gauge output and the moment distribution, a calibration of the

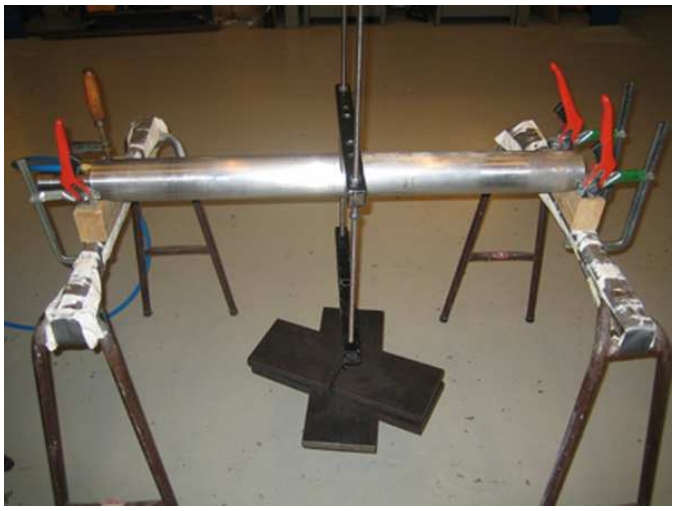

Figure 9: Test setup for calibration of pile bending stiffness, E_pI_p, and validation of strain gauges.

piles have been conducted by loading the piles transversely while supported as simply supported beams. In order to eliminate effects of stress concentrations, four load series with varying locations of the point load have been conducted at each pile. At each location load series consisting of seven load steps of 20 kg, from 0 – 120 kg have been applied. The setup is shown in fig. 9. An example of the test results is shown in fig. 10 for the upper strain gauge level. From Bernoulli–Euler beam theory the following relation between moment and strains is obtained:

$$E_pI_p = \frac{Mr^*}{\bar{\varepsilon}} \tag{1}$$

E_pI_p is the stiffness of the pile corresponding to the applied moment, M, and the mean value of the measured strains at a given strain gauge level, $\bar{\varepsilon}$. The slope of a linear regression to the points shown in fig. 10 is in accordance to (1) multiplied with the distance from the cross sectional centre to the gauge, $r^* = D/2 - t^*$, where D is the outer diameter of the pile and t^* is the depth of the mill out. Hereby, the pile bending stiffness, E_pI_p, is obtained. Similar interpretations have been made for each of the four other strain gauge levels. By taking the average of the bending stiffness' obtained at each strain gauge level the calibrated bending stiffness' of the piles are determined to $EI_{80,calibrated}$ =52.4 kNm^2 and $EI_{60,calibrated}$ =24.9 kNm^2 for the two pile diameters, respectively. The standard deviation are σ_{80}=0.874 and σ_{60}=0.585. Due to the small strains obtained at the strain gauge level nearest to the pile-toe, large uncertainties are introduced. The results obtained at this level have been omitted in the calculation of E_pI_p.

4 Soil conditions

The tests are conducted on fully saturated Baskarp Sand no. 15, with the characteristics given in tab. 1. The distribution of grain size determined from sieve analysis is shown in fig. 11.

Table 1: Material properties for Baskarp Sand no. 15, after Larsen (2008).

Specific grain density d_s	2.64
Maximum void ratio $e_{\max}$	0.858
Minimum void ratio $e_{\min}$	0.549
d_{50} = 50 % - quantile	0.14 mm
$U = d_{60}/d_{10}$	1.78

The Baskarp sand nr. 15 contains uniformly graded small grains which makes a homogenously compaction possible. The

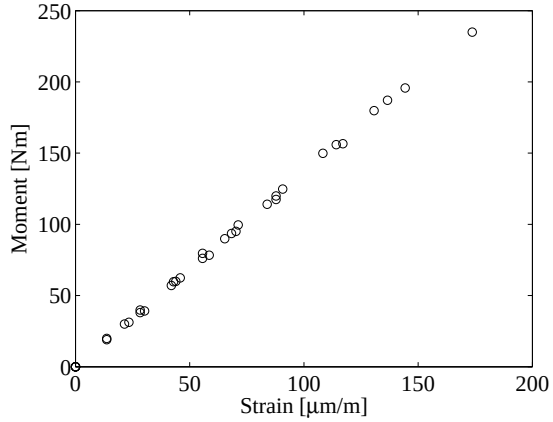

(a) $D = 80$ mm, $x = 5$ mm.

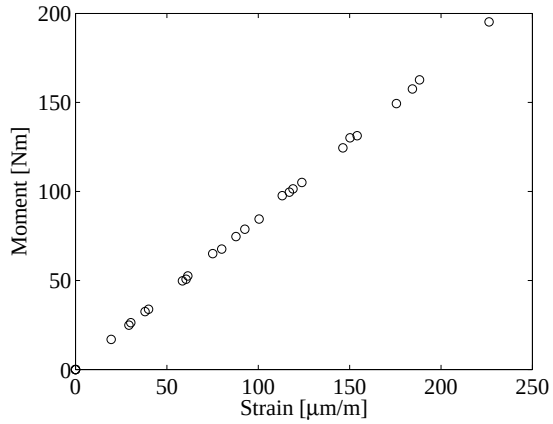

(b) $D = 60$ mm, $x = 0$ mm.

Figure 10: Measured strains versus applied moments at the upper strain gauge level.

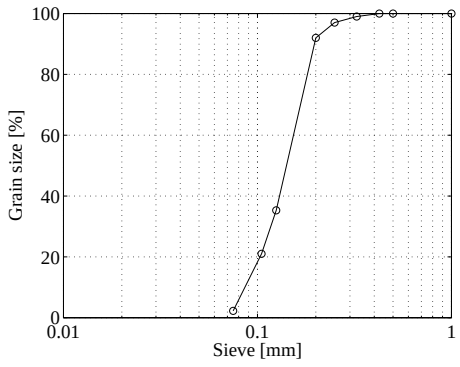

Figure 11: Distribution of grains for Baskarp Sand no. 15, after Larsen (2008).

sand is permeable with the hydraulic conductivity $k \approx 6 \cdot 10^{-5}$ m/s which allows drained conditions during the tests.

4.1 Preparation of soil

Between each test the soil is prepared by mechanical vibration. This ensures that the sand is fully saturated, and a homogeneous compaction of the material is obtained.

The piles are installed at the centre of the pressure tank, with the strain gauges aligned in the plane of the horizontal load. During installation an upward gradient of a magnitude of 0.9 has been applied in order to minimise the pressure at the closed pile-end and to protect the strain gauges. In this way the toe resistance and the skin friction along the pile are minimised during pile installation. After the installation of the pile the sand is mechanically vibrated minimising the disturbances from the pile installation, i.e. a homogeneous compaction of the sand is ensured. The pile is prevented from deforming from its upright position when vibrating with use of the hydraulic piston mounted on the top hatch, cf. ⑫ in fig. 2.

The compaction and homogeneity have been controlled by cone penetration tests (CPT). Four CPT's with a distance of 0.5 m from the centre of the pile and two at the neutral sides of the pile, i.e. the sides perpendicular to the load direction, with a distance of 0.16 m have been conducted. The employed CPT probe has a diameter of 15 mm.

A typical profile of the cone tip resistance, q_c, is shown in fig. 12a. The results from all tests are given in appendices I–N. As the profiles of q_c are without particular variation at the described six different locations in the pressure tank, the soil is considered homogenously compacted. Figure 12b presents the mean values of each series of six CPT's conducted prior to each

pile test. As shown the same compaction is reached prior to each test.

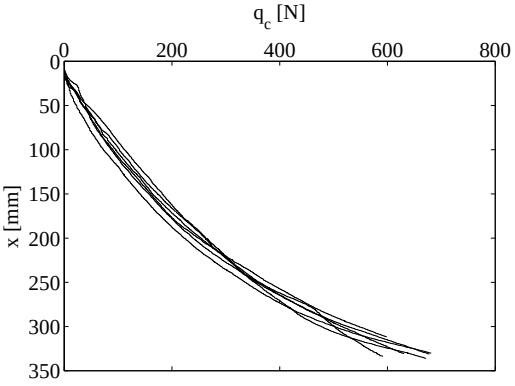

(a) Series of six CPT's prior to test nr. 2.

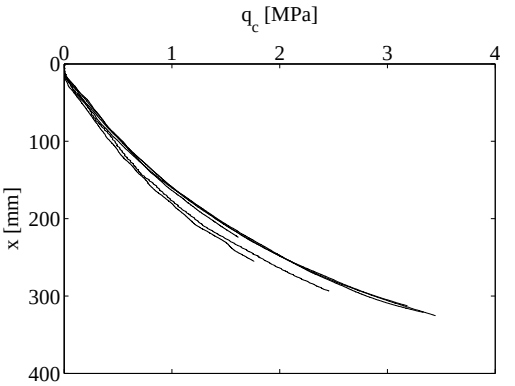

(b) Mean values of CPT's conducted prior to each test.

Figure 12: Output from CPT's.

Table 2: Material properties. P_0 denote the magnitude of the overburden pressure.

	P_0 [kPa]	φ_{tr} [°]	I_D [–]	γ' [kN/m^3]
Test 1	0	52.6	0.79	10.2
Test 2	100	45.9	0.79	10.2
Test 3	50	48.5	0.79	10.2
Test 4	0	52.2	0.76	10.1
Test 5	50	48.3	0.78	10.1
Test 6	100	45.1	0.75	10.1

Soil parameters derived on the basis of the CPT's are presented in tab. 2. The parameters are derived in accordance to Ibsen et al. (2009) where the angle of internal friction is related to the stress level.

5 Results

The test programme, cf. tab. 3, is designed to investigate the soil resistance and its dependency on pile diameter at different stress levels.

During the tests, the soil is brought to failure, unloaded, and reloaded in order to estimate the ultimate soil resistance and the elastic behaviour of the soil. The applied displacements are of varying magnitudes due to different overburden pressures, P_0, and pile diameters, D.

Table 3: Test programme. The vertical distances a and e are illustrated in fig. 5.

	D [mm]	L/D	a [m]	e [m]	P_0 [kPa]
Test 1	80	5	0.200	0.370	0
Test 2	80	5	0.200	0.370	100
Test 3	80	5	0.200	0.370	50
Test 4	60	5	0.205	0.375	0
Test 5	60	5	0.205	0.375	50
Test 6	60	5	0.205	0.375	100

Figure 13a presents the load-displacement relationship for test 4, cf. tab. 3, while the normalised load-displacement relationships for test 4–6 are shown in fig. 13b. The horizontal load, cf. fig. 13b, is normalised as H/H_{max} where H_{max} denotes the ultimate load at each test and the horizontal displacement is normalised with outer pile diameter, y/D. A low-pass filter with a cutoff frequency at 0.1 Hz has been employed. From fig. 13 it is seen that after the first unloading and reloading the load-displacement curves reaches the original curves. Furthermore, the upper displacement transducer produce the highest displacement and the lower displacement transducer produce the smallest displacement, which is as expected. The plastic behaviour of the soil is dependent on the amount of overburden pressure. After the first unloading the plastic deformation of the soil is determined to approximately 80% of the total deformation without over-

burden pressure, 60% of the total deformation when applying $P_0 = 50$ kPa, and 55% of the total deformation when applying $P_0 = 100$ kPa. However, it should be emphasised that the applied lateral deflection is larger for the tests without overburden pressure.

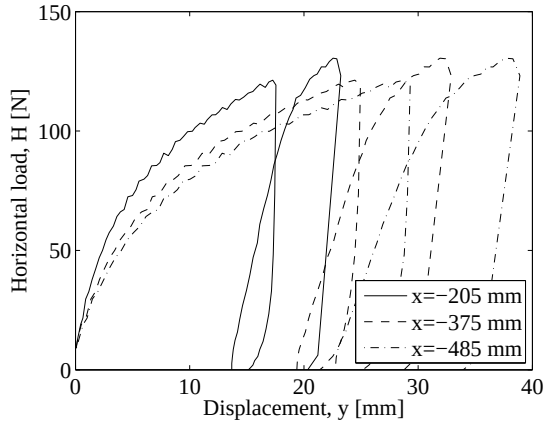

(a) $P_0 = 0$ kPa.

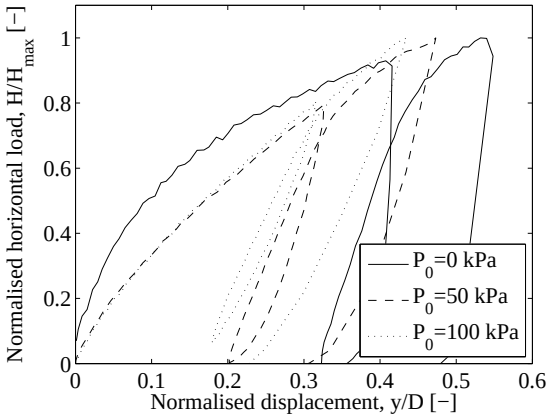

(b) Normalised relationships between load (H/H_{max}) and displacement (y/D) measured at the height of the hydraulic piston.

Figure 13: Load-displacement relationships for the pile with an outer diameter of 60 mm.

Figure 14 presents the dependency of overburden pressure on the lateral load. The required lateral loads in order to obtain a given pile displacement are, as expected, highly dependent of the magnitude of the overburden pressure. The lateral load at 10 mm deflection at the level of the hydraulic piston increases with a factor of approximately 20 and 13 for $D = 60$ and $D = 80$ mm, respectively at $P_0 = 50$ kPa. The factors increases to approximately 31 and 20 for $P_0 = 100$ kPa. These factors are determined in comparison with the loads without overburden pressure.

After a displacement of 20 mm, cf. fig. 14b, the load-displacement relationship for test 3 ($P_0 = 50$ kPa, $D = 80$ mm) is unrealistic as it recovers strength. This error might be caused by deviations in the pressure in the pressure tank. Hence, only the initial part of this test curve is valid. The deviations have only been only observed during test 3.

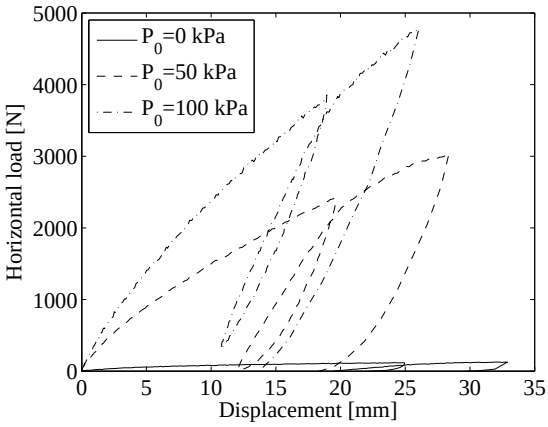

(a) $D = 60$ mm.

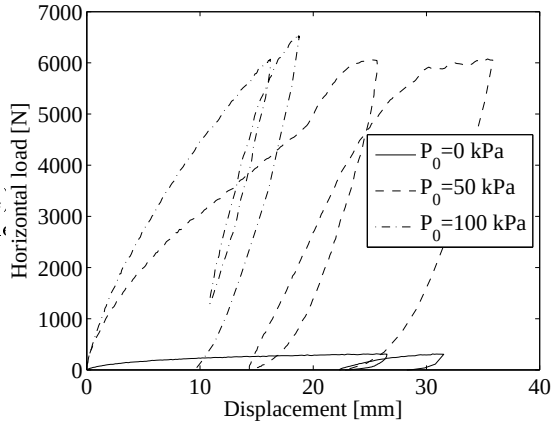

(b) $D = 80$ mm.

Figure 14: Load-displacement relationships at different overburden pressures measured at the height of the hydraulic piston.

The vertical displacement versus time until the first unloading is presented in fig. 15 for the pile with an outer diameter of 60 mm without overburden pressure. The

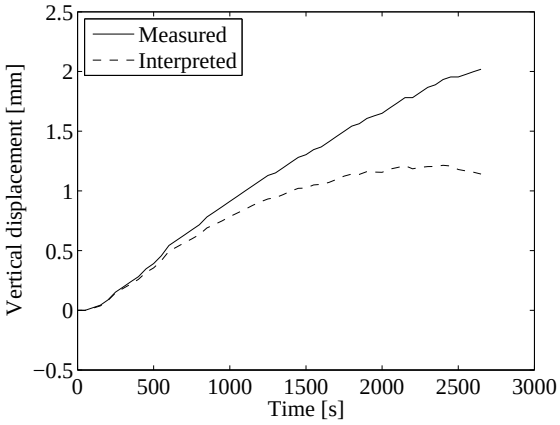

Figure 15: Vertical pile displacement versus time for $D = 60$ mm, and $P_0 = 0$ kPa. A positive vertical displacement indicate that the pile moves upward.

vertical displacement are measured at the back of the pile with a wire transducer, cf. fig. 5. Hereby, both the rotation of the pile as a rigid object and the pile deformation contributes to the measured values of the vertical displacements. These contributions are deducted with use of the laws of trigonometry. From fig. 15 an interpreted maximum vertical displacement of 1.2 mm is observed. This corresponds to 0.4 % of the embedded pile length and the effect of this on the soil-pile interaction is negligible. When applying overburden pressures the upward displacement is of the same magnitude as outlined in fig. 15.

5.1 Interpretation of strain gauge measurements

The strain gauge measurements are interpreted in order to derive p–y curves and the moment distributions along the piles. A mean value, $\overline{\varepsilon}$, of the strains is calculated for each level, and the curvature, κ, and bending moments, M, are calculated by:

$$\kappa = \frac{\overline{\varepsilon}}{r*} \tag{2}$$

$$M = E_p I_p \kappa \tag{3}$$

When interpreting the strain gauge measurements, zero curvature is assumed at the pile-toe. Hereby, the curvature is known in six levels of the piles. In order to calculate the pile deflection the discrete curvature measurements, κ, are fitted to a 5. order polynomial.

The deflection of the pile, y, and the soil resistance, p, are calculated from (4) and (5), respectively.

$$y(x) = \int\int \frac{M}{E_p I_p} dx dx \tag{4}$$

$$p(x) = \frac{d^2 M}{dx^2} \tag{5}$$

The double integration of moments with respect to depth, cf. (4), does not implement significant errors. However, double differentiation of the discrete moments results in an amplification of measurement errors. In order to minimise these errors the piecewise polynomial curve fitting method described by Yang and Liang (2006) is employed. The boundary conditions, cf. (4), for the pile deflection and rotation at the mudline are calculated based on displacements measured at the level of the hydraulic piston and 110 mm above, cf. fig. 5.

Figure 16 presents the bending moment distributions along the piles corresponding to the prescribed horizontal displacements listed in tab. 4. The maximum bending moment occurs at different locations depending on the magnitude of the overburden pressure. Without overburden pressure the depth of maximum bending moment is located at around 1/4 of the embedded pile length determined from the soil surface. The maximum moment is situated between 1/8 of the embedment length and the soil surface when applying overburden pressures. Therefore, it is concluded that the relative increase in soil resistance with overburden pressure is most significant at the soil surface.

Table 4: Applied displacements at the level of the hydraulic piston, and equivalent loads.

	D [mm]	P_0 [kPa]	Displacement [mm]	Load [N]
Test 1	80	0	30.7	311
Test 2	80	100	16.2	6071
Test 3	80	50	17.6	4457
Test 4	60	0	25.0	115
Test 5	60	50	19.6	2421
Test 6	60	100	18.9	3856

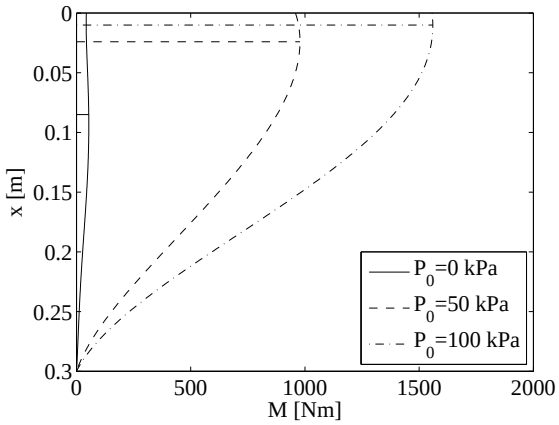

(a) $D = 60$ mm.

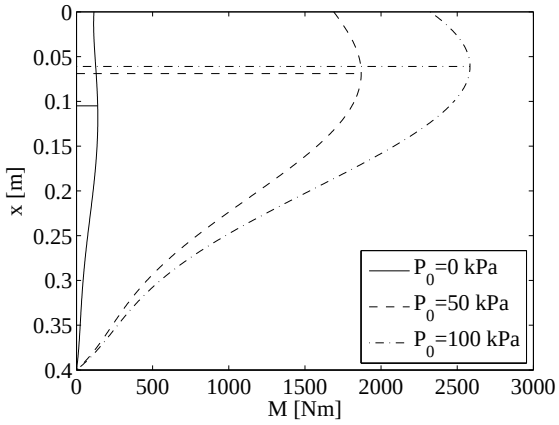

(b) $D = 80$ mm.

Figure 16: Bending moment distributions at different overburden pressures. The horizontal lines indicates the depth of maximum moment.

Figure 17 presents the pile lateral displacements with depth at the three overburden pressures for the two pile diameters. A prescribed displacement at the hydraulic piston of 10 mm has been applied. The lateral displacement can be separated into two components:

- Deformation of the pile due to bending moments.
- Rotation of the pile as a rigid body.

The pile deformation due to bending is determined in accordance to (4). The pile rotation above the hydraulic piston is obtained by the top two displacement transducers, cf. fig. 5. As shown in fig. 17, the pile exhibit an almost rigid body motion in the tests without overburden pressure. When applying overburden pressure the pile deformation caused by bending is more significant, but still with a pile deflection primarily depending on the rotation. Poulus and Hull (1989) proposed a criterion for the soil-pile interaction in which a high Young's modulus of elasticity for the soil in comparison with the stiffness of the pile material, leads to a flexible pile behaviour. When applying overburden pressure the effective stress level increases leading to an increase in Young's modulus of elasticity of the soil. Hereby, the more flexible pile behaviour for the tests with overburden pressure is as expected. Due to the rigid pile behaviour the deflection at the pile-toe must be negative which is not the case for most of the tests. This might be due to the relatively small vertical distance between the displacement transducers, cf. fig. 5, which leads to large uncertainties when determining the pile rotation.

Figure 18 presents normalised relationships between load, $H/L^2D\gamma'$, and displacement, y/D, determined at the height

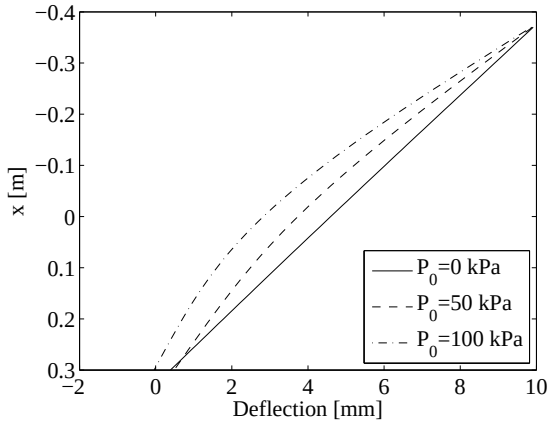

(a) $D = 60$ mm.

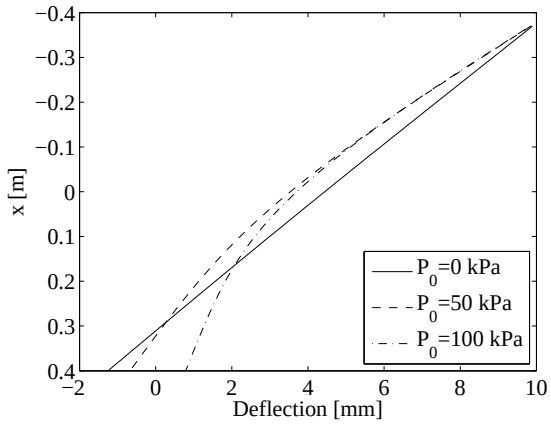

(b) $D = 80$ mm.

Figure 17: Lateral pile deflection at different overburden pressures.

of the hydraulic piston for the three stress levels. When overburden pressure is applied the initial part of the curves are very similar. This indicate that the lateral load is proportional to the embedded length squared and the pile diameter. Figure 18a indicate that the lateral load might be proportional to the pile diameter with a factor larger than one. It should be emphasised that the slenderness ratio is constant during the tests implying that the lateral load might as well be proportional to the embedded length and the pile diameter squared.

5.2 Comparison of test results with a traditional Winkler model approach

A traditional Winkler model has been constructed in order to compare the test results to the recommendations in the design regulations, e.g. API (1993) and DNV (1992). The Winkler model is made in *MATLAB* with use of the finite element toolbox *CALFEM*.

Figure 19 presents the load-displacement relationships for the tests without overburden pressure. Further, the relationships determined by means of the Winkler model are outlined in the figure. As expected the load increases with increasing pile diameter. The ultimate horizontal load given as the asymptotic horizontal value is overestimated, most significantly for $D = 80$ mm, when employing the recommendations in API (1993). However, for the initial part of the curves a good agreement between the Winkler model and the test results is observed until reaching a displacement of approximately 3 mm.

In order to evaluate the ultimate soil resistance presented in API (1993), load-displacement relationships are calculated using an upper bound solution for the ultimate soil resistance, cf. Jacobsen and Gwizdala (1992), and the formulation pro-

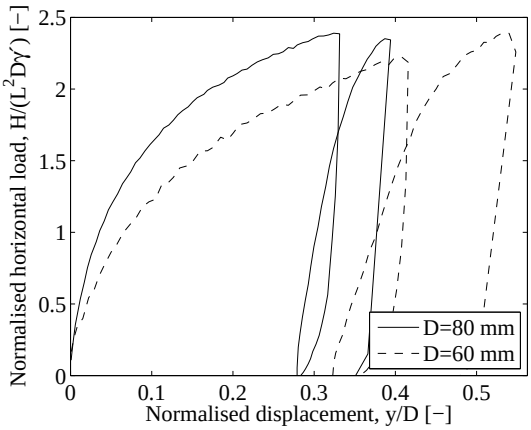

(a) $P_0 = 0$ kPa.

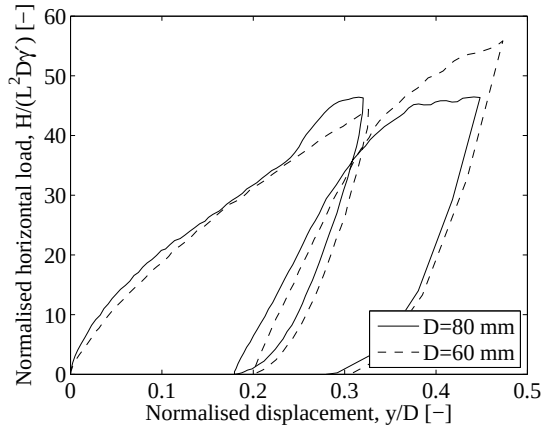

(b) $P_0 = 50$ kPa.

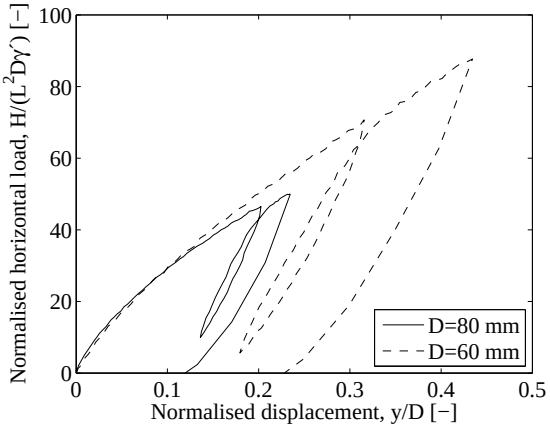

(c) $P_0 = 100$ kPa.

Figure 18: Normalised relationships between load ($H/L^2D\gamma'$) and displacement (y/D) determined at the height of the hydraulic piston.

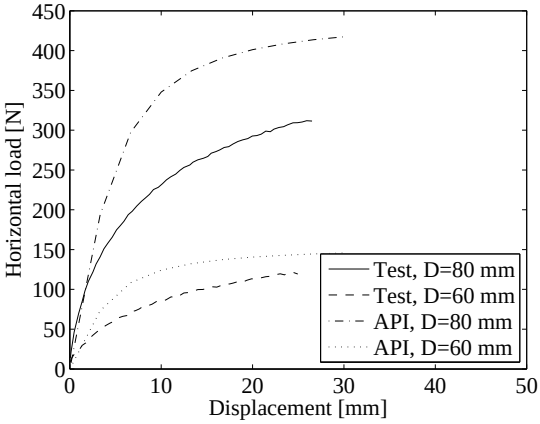

Figure 19: Comparison of measured load-displacement relationships at the height of the hydraulic piston with results obtained by means of a Winkler model approach. $P_0 = 0$ kPa. The initial modulus of subgrade reaction, k, is set to 40.000 kN/m^3 while the angles of internal friction are as listed in tab. 2.

posed by Hansen (1961). The distinction between the three methods is the spreading of the wedge forming in front of the pile. Load-displacement relationships for the three methods incorporated in the Winkler model, and the test results are presented in fig. 20 for the pile with an outer diameter of 80 mm and $P_0 = 0$ kPa. From the figure it is observed that the upper bound solution overestimates the ultimate resistance and that the formulation by Hansen (1961) underestimates the ultimate resistance. The best agreement to the current study is the method proposed in the design regulations. Similar results have been observed for the pile with an outer diameter of 60 mm. This is in contradiction to the investigation performed by Fan and Long (2005) in which Hansen's method was found to produce the most reliable results when predicting the ultimate soil resistance. However, the investigation by Fan and Long (2005) considered only slender piles with diameters between 0.3-1.2 m modelled in a finite element program. Furthermore, the investigation considered the ultimate soil resistance of the *p–y* curves until a depth of 2.5 m while the analysis above considers the

load-displacement relationship at the pile-head. On basis of the laboratory tests it is concluded that the determination of ultimate soil resistance in accordance to API (1993) is workable but non-conservative.

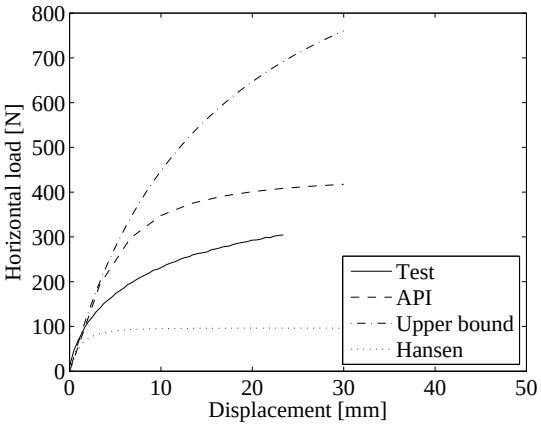

Figure 20: Load-displacement relationships determined at the height of the hydraulic piston versus three criterions, cf. API (1993), upper-bound, and Hansen (1961). $P_0 = 0$ kPa, $D = 80$ mm. The initial modulus of subgrade reaction, k, is set to 40.000 kN/m^3 while the angle of internal friction is as listed in tab. 2.

Figure 21 presents the derived p–y curves based on the tests and the p–y curves obtained by means of API (1993) at two strain gauge levels for each pile. The selected levels are located near the depth of the maximum moment and with strain gauge devices above and below. Hereby, the soil resistance is determined with good reliability for the chosen levels. In order to take the effect of overburden pressure, P_0, into account the approach described by Georgiadis (1983) is employed. In accordance to this an equivalent system with a fictive depth, x', is employed to describe the effect of the overburden pressure. The fictive depth varies between 0.41–0.71 m for the tests with overburden pressure. As shown in fig. 21c this method provides smaller variations of soil resistance than obtained by the tests. This is caused by the fact that x' is high compared to the distance between the single strain gauge levels. It should be emphasised that the employed method proposed by Georgiadis (1983) is for physically soil layers where friction between layers are taken into account. This is not the case when the overburden pressure is separated from the soil by the elastic membrane. Without overburden pressure the results obtained from the Winkler model approach, cf. fig. 21a, is closer to the test results, though with significant deviations.

Figure 22 presents normalised relationships between soil resistance, $p/D\sigma'$, and deflection, y/D, at two depths. The observations leads to the conclusion that the initial stiffness of the p–y curve is highly dependent on the pile diameter; the larger pile diameter the higher initial stiffness. In the case without overburden pressure the initial stiffness for the pile with an outer diameter of 80 mm is in the range of 3–4 times higher than the stiffness for the pile with an outer diameter of 60 mm. However, it should be emphasised that the p–y curves are obtained in different depths and at different embedded pile lengths. According to API (1993) the initial stiffness is independent on the pile diameter. This seems questionable based on this analyses. In the normalised figures the initial slope decreases when overburden pressures is applied. The factor is in the range of 7–30% of the slope without overburden pressures. However, it should be emphasised that the vertical stress distribution, cf. fig. 4, is abnormal for the tests with overburden pressures.

6 Conclusion

The paper presents the results of six quasi-static tests on laterally loaded monopiles. The tests are carried out in a pressure tank at varying effective stress levels from 0–100 kPa. When increasing the effective stresses in the soil, problems with a non-linear yield surface, as for small stress levels, are overcome. The tests are conducted on two aluminium pipe piles with outer di-

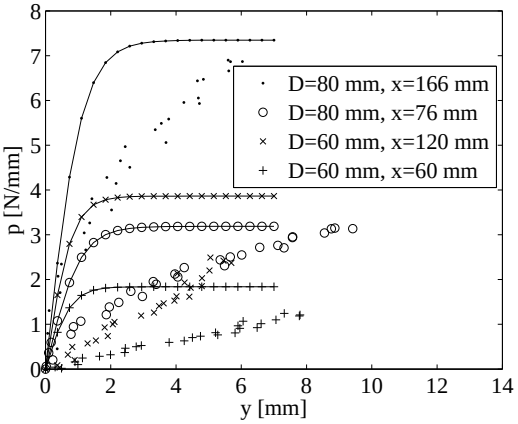

(a) $P_0 = 0$ kPa.

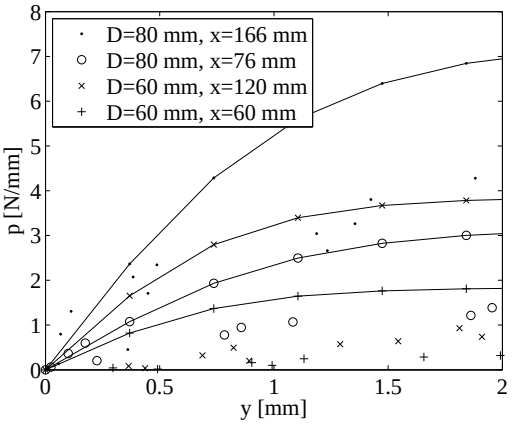

(b) Initial part of fig. 21a.

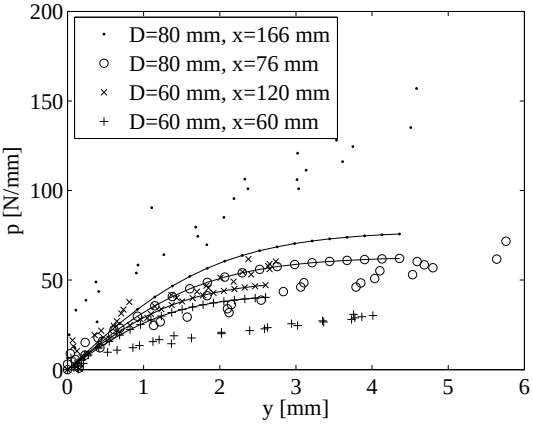

(c) $P_0 = 100$ kPa.

Figure 21: Derived p–y curves compared to the p–y curves recommended in API (1993). The solid lines denotes the p–y curves determined by the recommendations in API (1993). The initial modulus of subgrade reaction, k, is set to 40.000 kN/m^3 while the angles of internal friction are as listed in tab. 2

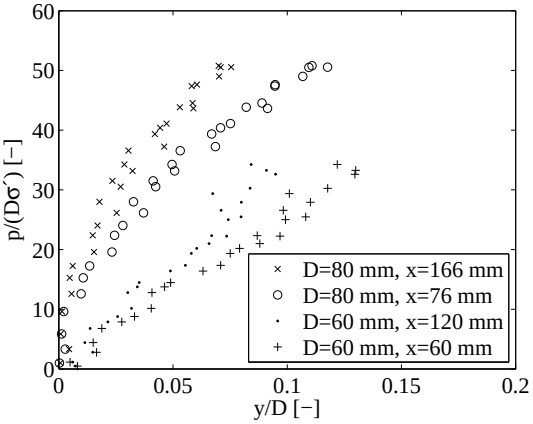

(a) $P_0 = 0$ kPa.

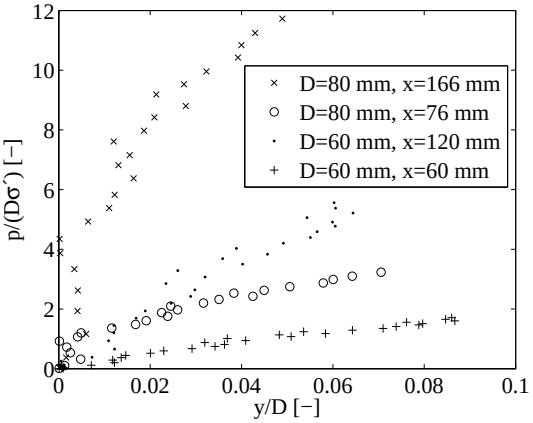

(b) $P_0 = 50$ kPa.

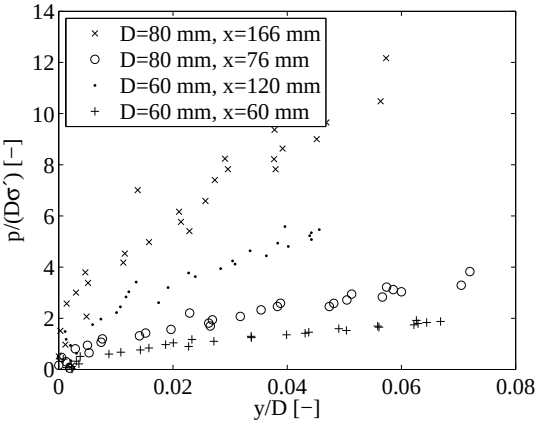

(c) $P_0 = 100$ kPa.

Figure 22: Normalised relationships between soil resistance ($p/D\sigma'$) and deflection (y/D) at different overburden pressures. σ' denote the effective vertical stress.

ameters of 80 mm and 60 mm. Both prototypes have a slenderness ratio, L/D, on 5. The piles are instrumented with a total of 10 strain gauges located at five levels along each pile.

The increase in effective stress level have been created by separating the lower part of the tank, containing saturated sand and pile, from the upper part by use of an elastic membrane. The test setup are working without any complications and the obtained results seems very reliable.

Based on the results obtained from the laboratory tests some conclusions may be drawn:

- The deflection of the piles consists primarily of a rigid body motion, i.e. the piles merely rotates around one point of zero deflection. This behaviour deviates from the behaviour of the slender piles tested at Mustang Island, which are the basis of the p–y relations employed in the design regulations, e.g. API (1993) and DNV (1992).

- When applying overburden pressures the soil resistance increases and as a consequence to this the piles exhibits a more flexible pile behaviour. Furthermore, the depth of the maximum moment moves closer to the soil surface when overburden pressure is applied.

- The tests indicate that the horizontal load acting at the pile-head is proportional to the embedded length squared and the pile diameter.

- The ultimate soil resistance determined by API (1993) provides a reasonable fit with the test results. The upper bound solution, cf. Jacobsen and Gwizdala (1992), and the method proposed by Hansen (1961) is not supported by the current study.

- The initial stiffness of the p–y curve is highly dependent on the pile diameter; the larger pile diameter the larger initial stiffness. This observation conflicts with the recommendations in the design regulations.

Acknowledgements

The project has only been possible with the financial support from the Energy Research Programme administered by the Danish Energy Authority. The project is associated with the EFP programme "Physical and numerical modelling of monopile for offshore wind turbines", journal no. 033001/33033-0039. The funding is sincerely acknowledged.

References

API, 1993. Recommended practice for planning, designing, and constructing fixed offshore platforms - Working stress design, *API RP2A-WSD*, American Petrolium Institute, Washington, D.C., 21. edition.

Cox W. R., Reese L. C., and Grubbs B. R., 1974. Field Testing of Laterally Loaded Piles in Sand. *Proceedings of the Sixth Annual Offshore Technology Conference*, Houston, Texas, paper no. OTC 2079.

DNV, 1992. Foundations - Classification Notes No 30.4, Det Norske Veritas, Det Norske Veritas Classification A/S.

Georgiadis M., 1983. Development of p–y curves for layered soils. *Proceedings of the Geotechnical Practice in Offshore Engineering*, ASCE, pp. 536-545.

Hansen B. J., 1961. *The ultimate resistance of rigid piles against transversal forces.* Danish Geotechnical Institute, Bull. No. 12, Copenhagen, Denmark, 5-9.

Ibsen L. B., Hanson M., Hjort T. H., and Thaarup M., 2009. MC–Parameter Calibration for Baskarp Sand No. 15. *DCE Technical Report No. 62*, Department of Civil Engineering, Aalborg University, Denmark.

Jacobsen M., and Gwizdala K., 1992. *Bearing Capacity and Settlements of Piles*. Centertrykkeriet, Aalborg University, Denmark.

Larsen K. A., 2008. Static Behaviour of Bucket Foundations. *DCE Thesis no. 7*, Department of Civil Engineering, Aalborg University, Denmark.

Poulus H., and Hull T., 1989. The Role of Analytical Geomechanics in Foundation Engineering. *in Foundation Eng.: Current principles and Practices*, **2**, pp. 1578-1606.

Yang K., Liang R., 2006. Methods for Deriving *p–y* Curves from Instrumented Lateral Load Tests. *Geotechnical Testing Journal*, **30**(1), paper ID GTJ100317, pp. 31-38.

ISSN 1901-726X
DCE Technical Report No. 79